ACS Photonics

Letter

pubs.acs.org/journal/apchd5

Monolithically Integrated InAs/GaAs Quantum Dot Mid-Infrared Photodetectors on Silicon Substrates

Jiang Wu,*[,†] Qi Jiang,[†] Siming Chen,[†] Mingchu Tang,[†] Yuriy I. Mazur,[‡] Yurii Maidaniuk,[‡] Mourad Benamara,[‡] Mykhaylo P. Semtsiv,[§] W. Ted Masselink,[§] Kimberly A. Sablon,[∥] Gregory J. Salamo,[‡] and Huiyun Liu[†]

[†]Department of Electronic and Electrical Engineering, University College London, London WC1E 7JE, United Kingdom

[‡]Institute for Nanoscience and Engineering, University of Arkansas, Fayetteville, Arkansas 72701, United States

[§]Physics Department, Humboldt University Berlin, Newtonstraße 15, 12489 Berlin, Germany

[∥]United States Army Research Laboratory, 2800 Powder Mill Road, Adelphi, Maryland 20783-1197, United States

ABSTRACT: High-performance, multispectral, and large-format infrared focal plane arrays are the long-demanded third-generation infrared technique for hyperspectral imaging, infrared spectroscopy, and target identification. A promising solution is to monolithically integrate infrared photodetectors on a silicon platform, which offers not only low-cost but high-resolution focal plane arrays by taking advantage of the well-established Si-based readout integrated circuits. Here, we report the first InAs/GaAs quantum dot (QD) infrared photodetectors monolithically integrated on silicon substrates by molecular beam epitaxy. The III−V photodetectors are directly grown on silicon substrates by using a GaAs buffer, which reduces the threading dislocation density to ~10^6 cm^{-2}. The high-quality QDs grown on Si substrates have led to long photocarrier relaxation time and low dark current density. Mid-infrared photodetection up to ~8 μm is also achieved at 80 K. This work demonstrates that III−V photodetectors can directly be integrated with silicon readout circuitry for realizing large-format focal plane arrays as well as mid-infrared photonics in silicon.

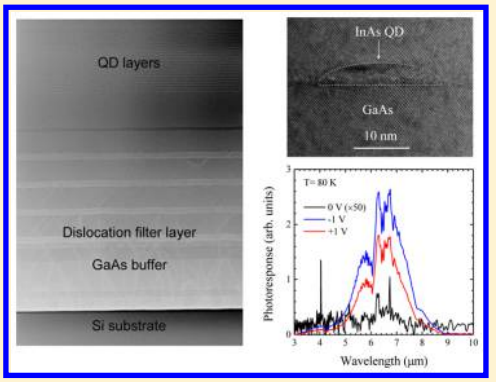

KEYWORDS: *quantum dots, infrared photodetectors, silicon, molecular beam epitaxy*

Infrared photodetectors can be applied to a wide range of applications, including free-space communication, surveillance, tracking and missile interception, chemical sensing, and biomedical imaging.[1] Until now, high-performance infrared photodetectors have been demonstrated in HgCdTe film, InGaAs/GaAs quantum wells (QWs), In(Ga)As/GaAs quantum dots (QDs), and InAs/GaSb type-II superlattice.[2−6] However, these devices require complicated fabrication steps and hybrid integration with silicon readout integrated circuits (ROICs), which limits the yield, performance, and format size.[7] The monolithic integration of photodetectors with Si ROICs can potentially result in faster speed, higher performance, enhanced functionality, and higher resolution focal plane arrays (FPAs).[8] There is also no doubt that it will dramatically reduce the fabrication cost using the standard silicon fabrication. This is particularly true for HgCdTe-based FPAs, which lack a low cost and high-quality substrates. The lattice-matched CdZnTe substrates are about \$200/cm^2 and limited to small size (7 × 7 cm^2).[9] Although Si is a promising substrate for large-format FPAs, the very large lattice mismatch (~19%) and thermal expansion coefficient (TEC) mismatch (~80%) between Si and HgCdTe present a great challenge for integration.[10]

Compared with HgCdTe alloys, III−V semiconductors, well-established infrared materials, have a similar TEC mismatch but distinctly reduced lattice mismatch to Si (~4%), which makes III−V materials promising alternatives for monolithically integrated FPAs on Si substrates. Among various techniques, QD infrared photodetectors (QDIPs) present several attractive merits, including high-temperature operation, low dark current, and high detectivity.[11−13] More importantly, carrier localization in QDs results in less sensitivity to defects and reduced negative influence of defects compared with conventional bulk materials and QW structures for III−V devices integrated on silicon platforms.[14,15] The strong strain fields generated by the QD arrays also restrict the movement of dislocations and, thus, further reduce the interaction between photogenerated carriers.[16] These unique properties of QDs have led to successful monolithic integration of III−V light sources on group IV substrates.[17−23]

In this paper, an InAs/GaAs QDIP has been directly grown on Si substrates. A GaAs buffer with a few sets of strained layer superlattices (SLSs) has been employed to overcome the high threading dislocation density induced by the lattice and TEC mismatch. High-quality GaAs/Si virtual substrates with low threading dislocation density on the order of ~10^6 cm^{-2} have

Received: February 2, 2016
Published: April 26, 2016

DOI: 10.1021/acsphotonics.6b00076
ACS Photonics 2016, 3, 749−753

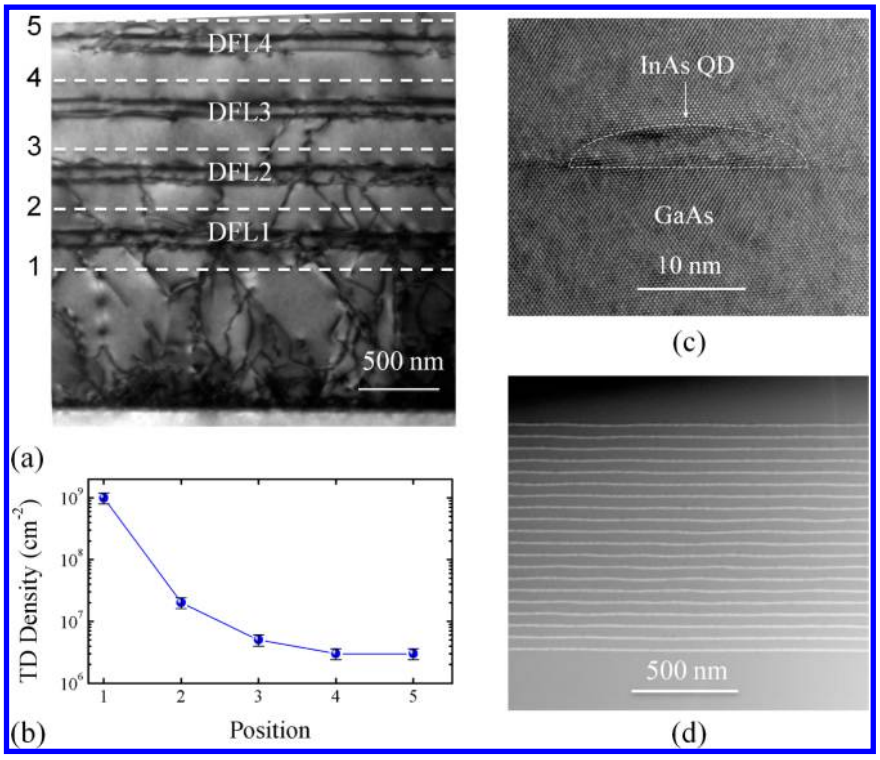

Figure 1. (a) Bright field multibeam TEM image showing threading dislocation reduction induced by dislocation filter layers (DFLs). (b) Estimated threading dislocations from TEM measurements at different positions in the GaAs buffer as indicated in (a). (c) Representative high-resolution TEM image of a single InAs/GaAs QD grown on the Si substrate. (d) Low-magnification bright field scanning TEM images of 20 layers of QDs grown on the Si substrate.

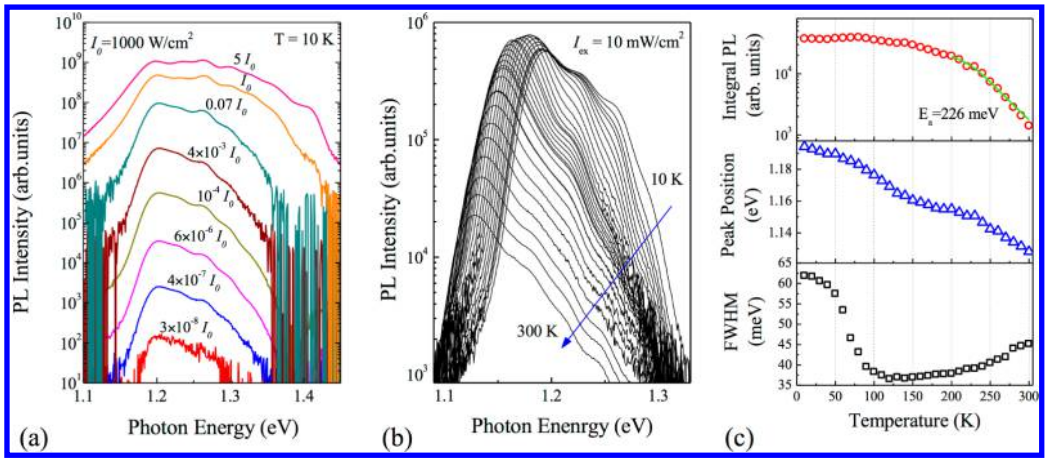

Figure 2. (a) PL spectra of the QDIP measured at 10 K under different excitation powers. I_0 = 1000 W/cm^2. (b) Temperature-dependent PL spectra of the QDIP measured from 10 to 300 K with an interval of 10 K at a laser excitation power of I_{ex} = 10 mW/cm^2. (c) Extracted PL parameters (integrated PL intensity, peak energy, and fwhm) as a function of temperature. The activation energy is estimated to be 226 ± 27.3 meV by fitting the integrated PL intensity in the temperature range between 200 and 300 K.

been obtained for the growth of QDIPs. Photodetection up to ~8 μm via transitions from the localized QD states to the conducting continuum (quasi-continuum) states is achieved at 80 K. A low dark current of 8.9 × 10^{-4} A/cm^2 (at 60 K and 1 V) is measured from the QDIPs, which is comparable to those reported for detectors grown on native substrates. This approach realizes the reliable and cost-effective monolithic integration of III−V devices on Si substrates. The demonstration of QDIPs monolithically integrated on Si substrates paves the way to realize large-format infrared FPAs as well as toward cost-effective mid-infrared Si photonics.

The GaAs buffer and QDIP active layers were directly grown on Si substrates by a solid-source Veeco Gen-930 molecular beam epitaxy system. To avoid formation of antiphase domains, 3 in. Si(100) wafers with 4° offcut toward the [011] direction were used. The Si wafers were thermally treated in ultrahigh vacuum at 900 °C for 30 min to remove any oxide formed on the surface before initialization of growth. A 5 nm AlAs nucleation layer was first deposited on the Si substrate at 370 °C by the migration-enhanced epitaxy. Sequentially, a GaAs buffer that consists of low-temperature GaAs and InGaAs/GaAs SLSs was grown. The buffer layer is the same as that reported in a previous study, except that four sets of InGaAs/GaAs SLSs

DOI: 10.1021/acsphotonics.6b00076
ACS Photonics 2016, 3, 749−753

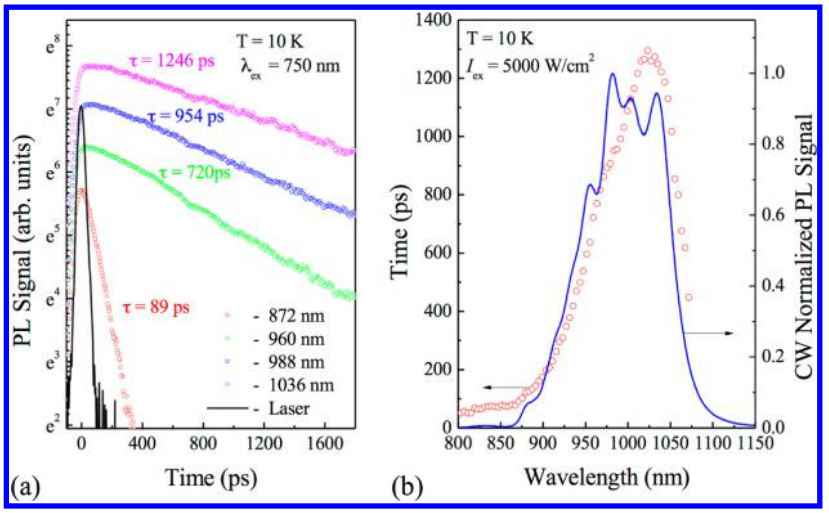

Figure 3. (a) PL decay transients measured at 10 K for different emission wavelengths: 872, 960, 988, and 1036 nm. (b) Estimated PL decay time (open circles) over the wavelength range of the PL spectrum. The blue curve is the PL spectrum measured at 10 K under a high laser excitation power of 5000 W/cm^2.

were used as threading dislocation filter layers.[24] Figure 1 shows the transmission electron microscopy (TEM) measurements of the GaAs buffer directly grown on Si substrates. As expected, a high density of threading dislocations is formed at the interface of the GaAs buffer and Si substrate as a result of their lattice and TEC mismatch. Despite that a large number of threading dislocations are self-annihilated in the first few hundred nanometers of GaAs buffer, a high threading dislocation density of 10^9 cm^{-2} can still be measured after growing 1 μm GaAs buffer. As shown in Figure 1a and b, the insertion of the SLSs significantly accelerates the annihilation of threading dislocations. After four sets of SLSs, the threading dislocations are reduced by 3 orders of magnitude and approximately reach the level of 10^6 cm^{-2}, which can no longer be accurately determined by the cross-sectional TEM (Figure 1b).

On the GaAs buffer, growth of QDIPs was then carried out as follows: a 500 nm n-type GaAs bottom contact layer (Si-doped, 2×10^{18} cm^{-3}), a 80 nm undoped GaAs spacer layer, 20 periods of InAs/GaAs QDs separated by 50 nm GaAs spacers, a second 80 nm undoped GaAs spacer layer, and a 300 nm n-type GaAs top contact layer (Si-doped, 2×10^{18} cm^{-3}). Each QD layer consisted of 2.1 monolayers (MLs) of InAs QDs. The QD layers were grown at 510 °C. Figure 1c shows a representative cross-sectional TEM image of a single InAs/GaAs QD grown on the Si substrate. A disc-shaped QD with dimension of 25 nm × 5 nm (diameter × height) is similar to that grown on GaAs substrates. Figure 1d shows a low-magnification bright field TEM image of the QDIP active layers, which presents a totally dislocation-free region of the 20 layers of QDs.

To gain insight into the optical properties and electronic structure of QDs directly grown on Si substrates, photoluminescence (PL) measurements were carried out using a Nd:YAG laser (532 nm excitation) with a laser spot diameter of 20 μm and a diode-pumped solid-state laser. Figure 2a presents the PL spectra measured under different excitation power intensities at 10 K. A broad emission peak at ∼1.2 eV attributed to the QD exciton ground state is measured at the lowest excitation intensity I_{ex} = 30 μW/cm^2. The full width at half-maximum (fwhm) of the peak is about 62 meV. Despite very low excitation power intensity, the peak is clearly asymmetric and cannot be fit by a single Gaussian function. With increasing excitation power, additional peaks appear on the high-energy side of the PL spectra, corresponding to emission from the excited states due to state filling at high optical excitation. The broad PL peak at ∼1.2 eV remains nearly unchanged with increasing excitation power until relative high excitation intensity I_{ex} > 1 W/cm^2, when a second peak emerges at ∼1.23 eV. Therefore, the broad and asymmetric PL peak at ∼1.2 eV may reflect an inhomogeneous size distribution of the QDs, particularly a bimodal size distribution.

Figure 2b and c show the temperature-dependent PL spectra and the extracted PL information (integrated PL intensity, peak energy, and fwhm), respectively. The PL peak experiences a typical red-shift but does not follow Varshini's equation. Such a behavior indicates carrier transfer from smaller QDs with shallower confinement to larger QDs with a deeper potential well with increasing temperature.[25] The carrier transfer process can also be reflected from the fwhm values as a function of temperature. A reduction of PL fwhm is observed until 100 K. This reduction is caused by the thermal repopulation of larger QDs from carrier transfer from small QDs.[20] On the other hand, the PL fwhm increases as a result of carrier scatter over QDs of different sizes with further increasing the temperature over 100 K.[26] In Figure 3c, the temperature-dependent integrated PL intensity shows the onset of the thermal PL quenching at around 200 K. By fitting the integrated PL intensity over 200 K, the activation energy, approximately the energy difference between the electron ground state and GaAs conduction band, is estimated to be 226 ± 27.3 meV. Except for the thermal PL quenching, no other PL quenching channels, e.g., nonradiative carrier recombination from defect/trap states, can be explicitly seen from the temperature-dependent PL measurements.

To further probe the quality of QDs grown on a Si substrate, transient PL measurements were performed using 2 ps pulses of 750 nm excitation from a mode-locked Ti:sapphire laser that produces an optical pulse train at 76 MHz and a Hamamatsu Synchroscan C5680 streak camera with an infrared enhanced S1 cathode. The laser excitation density per pulse was 6×10^{11} photons/cm^2. Figure 3a shows the PL transients measured at 10 K for different detection wavelengths. Figure 3b plots the extracted decay time at each wavelength overlaid with the PL

DOI: 10.1021/acsphotonics.6b00076
ACS Photonics 2016, 3, 749−753

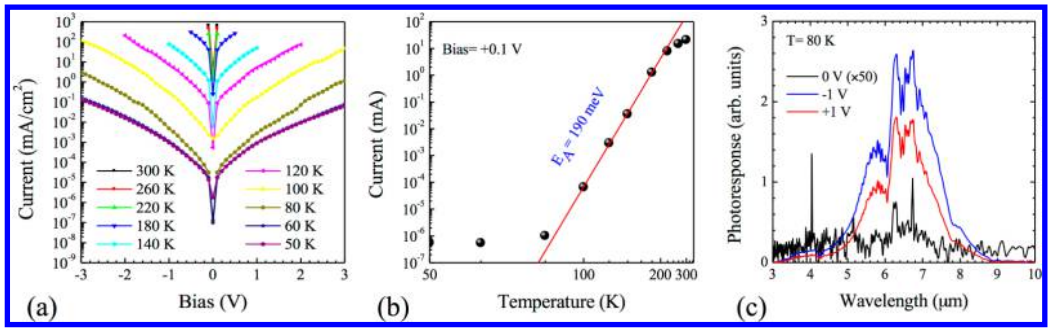

Figure 4. (a) Dark IV characteristics at different temperatures for the InAs/GaAs QDIP directly grown on the Si substrate. (b) Dark current activation energy extracted from the dark current measured under a bias voltage of 0.1 V. The fitting error is 1.9 meV. (c) Photocurrent spectra measured with different bias voltages at 80 K.

spectrum measured at a high excitation density of 5000 W/cm^2. As shown in Figure 3a, all the PL transients have a relatively long decay time over 500 ps, except the emission from the wetting layer measured at ∼872 nm (∼89 ps). All PL peaks from the QDs displayed in Figure 3b have shown quite slow PL decay (>500 ps). Particularly, the decay time for the ground-state transition is as long as ∼1.3 ns, which is comparable to the typical values reported for InAs QDs grown on GaAs substrates.[27] The long decay time signals that the dominant PL decay for the QD states is radiative recombination.[28] Therefore, the long-lived PL in the QDs suggests the GaAs buffer technique used here provides a high-quality QDIP with low defect density.

The QDIPs were fabricated into circular mesas by standard photolithography and wet chemical etching techniques. Mesas were fabricated with different diameters from 25 μm to 1 mm. Ni/GeAu/Ni/Au were deposited on both bottom and top n$^+$-GaAs contact layers. Rapid thermal annealing was then applied to form the ohmic contacts. The dark current is one of the key factors that restrict the performance of photodetectors. A low dark current level of photodetectors can withstand the detrimental thermal effects, e.g., thermionic emission, at higher operating temperatures. The temperature-dependent dark current−voltage characteristics of the QDIP on Si substrates are plotted in Figure 4a. The dark current density experience considerable increase with bias and temperature due to the field-assisted tunneling and thermionic emission, respectively. Nonetheless, a rather low dark current density (8.9×10^{-4} A/cm^2 at 60 K and 2.8×10^{-3} A/cm^2 at 80 K, both at 1 V) is measured from the QDIP directly grown on a Si substrate. Despite the presence of threading dislocations (∼10^6 cm^{-2}) caused by the large lattice and TEC mismatch, the QDIP on Si shows comparable dark current density to state-of-the-art devices grown on a native substrate.[29] It should be noted that no current-blocking layer, which can provide further reduction in dark current, has been used in this study. The temperature-dependent dark current in Figure 4b provides the dark current activation energy, which is fitted as ∼190 ± 1.9 meV. Compared with the PL quenching activation energy of 226 ± 27.3 meV, this value is slightly lower. It should be noted that the dark current data show the activation energy for photoelectrons, but PL measurements are based on electron−hole recombination and show the sum of activation energies of electrons and holes.[30,31] Therefore, the difference of ∼36 meV is the hole activation energy.

The photocurrent spectra of the QDIP were acquired with a Bruker Equinox-55 Fourier-transform spectrometer in the normal incidence configuration at different applied bias voltages at 80 K. The mesa size of the QDIP is 1 mm in diameter. A glow-bar infrared light source is normal incident on the device. The photocurrent signal was amplified using the SR570 low-noise current preamplifier by Stanford Research Systems. This preamplifier has also provided an electrical bias for the QDIPs. The amplified signal was ac-coupled to a spectrometer to cut off the dark current signal. Figure 4c plots the photoresponse spectra of the QDIP covering a broadband spectral range from 5 to 8 μm. The broad photoresponce spectra acquired at +1 V and −1 V are overlaid by sharp absorption lines of residual atmospheric moisture in the spectrometer. The sharp peaks in the spectrum acquired at 0 V are artifacts and have to be discarded. The photoresponse main peak (λ_p) is about 6.5 μm (190.7 meV) with an fwhm ($\Delta\lambda$) of 2.0 μm. The broad photoresponse ($\Delta\lambda/\lambda_p$ = 30.7%) suggests transitions from QD bound states to continuum states. In addition, the corresponding energy (190.7 meV) of the photoresponse peak is in good agreement with the activation energy extracted from the dark current measurements, which supports bound-to-continuum transitions in the QDIP. The photoresponse intensity measured at negative bias voltage is slightly higher than that at positive bias voltage. This behavior can be explained by the inherent asymmetry of the self-assembled QDs grown by the Stranski−Krastanov mode. A built-in electric field is normally present in the QD device as a result of the existence of the wetting layer, the asymmetric shape of the QDs, and anisotropic strain distribution.[32] The built-in electric field also leads to a slight asymmetry of the dark IV (Figure 4a) and the photoresponse measured at zero bias voltage (Figure 4c).

In conclusion, we present the first direct growth of mid-infrared InAs/GaAs QDIPs on Si substrates by molecular beam epitaxy. High-quality InAs/GaAs QDs have been realized on Si substrates by optimizing the GaAs buffer layers on Si substrates. The GaAs buffer presents a low threading dislocation density of ∼10^6 cm^{-2}. A long PL decay time up to 1.3 ns has been measured from the QDs grown on Si, indicating that high-quality QDIPs can be directly grown on Si substrates. The high-quality QDs grown on Si lead to observation of photocurrent in the mid-infrared spectral range from 5 to 8 μm due to optical transitions from the localized QD states to the conducting continuum (or quasi-continuum) states. The low dark current density of 8.9×10^{-4} A/cm^2 (at 1 V) also confirms the high quality of the III−V optoelectronic materials directly grown on Si substrates.

AUTHOR INFORMATION

Corresponding Author

*E-mail: jiang.wu@ucl.ac.uk (J. Wu).

DOI: 10.1021/acsphotonics.6b00076
ACS Photonics 2016, 3, 749−753

Notes

The authors declare no competing financial interest.

■ ACKNOWLEDGMENTS

The authors acknowledge the support of the National Science Foundation of the U.S. (EPSCoR Grant No. OIA-1457888). H.L. would like to thank The Royal Society for funding his University Research Fellowship.

■ REFERENCES

(1) Razeghi, M.; Nguyen, B. Advances in mid-infrared detection and imaging: a key issues review. *Rep. Prog. Phys.* **2014**, *77*, 082401.
(2) Itsuno, A. M.; Phillips, J. D.; Velicu, S. Mid-wave infrared HgCdTe nBn photodetector. *Appl. Phys. Lett.* **2012**, *100*, 161102.
(3) Hinds, S.; Buchanan, M.; Dudek, R.; Haffouz, S.; Laframboise, S.; Wasilewski, Z.; Liu, H. Near-Room-Temperature Mid-Infrared Quantum Well Photodetector. *Adv. Mater.* **2011**, *23*, 5536−5539.
(4) Lee, S. J.; Ku, Z.; Barve, A.; Montoya, J.; Jang, W.; Brueck, S. R. J.; Sundaram, M.; Reisinger, A.; Krishna, S.; Noh, S. K. A monolithically integrated plasmonic infrared quantum dot camera. *Nat. Commun.* **2011**, *2*, 286.
(5) Wu, J.; Shao, D.; Dorogan, V. G.; Li, A. Z.; Li, S.; Decuir, E. A.; Manasreh, M. O.; Wang, Z. M.; Mazur, Y. I.; Salamo, G. J. Intersublevel Infrared Photodetector with Strain-Free GaAs Quantum Dot Pairs Grown by High-Temperature Droplet Epitaxy. *Nano Lett.* **2010**, *10*, 1512−1516.
(6) Gautam, N.; Kim, H.; Kutty, M.; Plis, E.; Dawson, L.; Krishna, S. Performance improvement of longwave infrared photodetector based on type-II InAs/GaSb superlattices using unipolar current blocking layers. *Appl. Phys. Lett.* **2010**, *96*, 231107.
(7) Wang, J.; Zens, T.; Hu, J.; Becla, P.; Kimerling, L. C.; Agarwal, A. M. Monolithically integrated, resonant-cavity-enhanced dual-band mid-infrared photodetector on silicon. *Appl. Phys. Lett.* **2012**, *100*, 211106.
(8) Konstantatos, G.; Sargent, E. H. Nanostructured materials for photon detection. *Nat. Nanotechnol.* **2010**, *5*, 391−400.
(9) Simingalam, S.; VanMil, B. L.; Chen, Y.; DeCuir, E. A.; Meissner, G. P.; Wijewarnasuriya, P.; Dhar, N. K.; Rao, M. V. Development and fabrication of extended short wavelength infrared HgCdTe sensors grown on CdTe/Si substrates by molecular beam epitaxy. *Solid-State Electron.* **2014**, *101*, 90−94.
(10) Lei, W.; Gu, R.; Antoszewski, J.; Dell, J.; Faraone, L. GaSb: A New Alternative Substrate for Epitaxial Growth of HgCdTe. *J. Electron. Mater.* **2014**, *43*, 2788−2794.
(11) Lim, H.; Tsao, S.; Zhang, W.; Razeghi, M. High-performance InAs quantum-dot infrared photodetectors grown on InP substrate operating at room temperature. *Appl. Phys. Lett.* **2007**, *90*, 131112.
(12) Wang, S.; Lin, S.; Wu, H.; Lee, C. Low dark current quantum-dot infrared photodetectors with an AlGaAs current blocking layer. *Appl. Phys. Lett.* **2001**, *78*, 1023−1025.
(13) Kim, E.; Madhukar, A.; Zhengmao, Y.; Campbell, J. C. High detectivity InAs quantum dot infrared photodetectors. *Appl. Phys. Lett.* **2004**, *84*, 3277−3279.
(14) Ribbat, C.; Sellin, R.; Grundmann, M.; Bimberg, D.; Sobolev, N.; Carmo, M. Enhanced radiation hardness of quantum dot lasers to high energy proton irradiation. *Electron. Lett.* **2001**, *37*, 174−175.
(15) Ledentsov, N. Quantum dot lasers: the birth and future trends. *Semiconductors* **1999**, *33*, 946−950.
(16) Beanland, R.; Sanchez, A.; Childs, D.; Groom, K.; Liu, H.; Mowbray, D.; Hopkinson, M. Structural analysis of life tested 1.3 μm quantum dot lasers. *J. Appl. Phys.* **2008**, *103*, 014913.
(17) Chen, S.; Tang, M.; Wu, J.; Jiang, Q.; Dorogan, V.; Benamara, M.; Mazur, Y.; Salamo, G.; Seeds, A.; Liu, H. 1.3 μm InAs/GaAs quantum-dot laser monolithically grown on Si substrates operating over 100 C. *Electron. Lett.* **2014**, *50*, 1467−1468.
(18) Jiang, Q.; Tang, M.; Chen, S.; Wu, J.; Seeds, A.; Liu, H. InAs/GaAs quantum-dot superluminescent diodes monolithically grown on a Ge substrate. *Opt. Express* **2014**, *22*, 23242−23248.
(19) Liu, A. Y.; Zhang, C.; Norman, J.; Snyder, A.; Lubyshev, D.; Fastenau, J. M.; Liu, A. W.; Gossard, A. C.; Bowers, J. E. High performance continuous wave 1.3 μm quantum dot lasers on silicon. *Appl. Phys. Lett.* **2014**, *104*, 041104.
(20) Tang, M.; Chen, S.; Wu, J.; Jiang, Q.; Dorogan, V. G.; Benamara, M.; Mazur, Y. I.; Salamo, G. J.; Seeds, A.; Liu, H. 1.3-μm InAs/GaAs quantum-dot lasers monolithically grown on Si substrates using InAlAs/GaAs dislocation filter layers. *Opt. Express* **2014**, *22*, 11528−11535.
(21) Wang, T.; Liu, H.; Lee, A.; Pozzi, F.; Seeds, A. 1.3-μm InAs/GaAs quantum-dot lasers monolithically grown on Si substrates. *Opt. Express* **2011**, *19*, 11381−11386.
(22) Liu, H.; Wang, T.; Jiang, Q.; Hogg, R.; Tutu, F.; Pozzi, F.; Seeds, A. Long-wavelength InAs/GaAs quantum-dot laser diode monolithically grown on Ge substrate. *Nat. Photonics* **2011**, *5*, 416−419.
(23) Liu, A. Y.; Herrick, R. W.; Ueda, O.; Petroff, P. M.; Gossard, A. C.; Bowers, J. E. Reliability of InAs/GaAs Quantum Dot Lasers Epitaxially Grown on Silicon. *IEEE J. Sel. Top. Quantum Electron.* **2015**, *21*, 690−697.
(24) Chen, S.; Tang, M.; Jiang, Q.; Wu, J.; Dorogan, V. G.; Benamara, M.; Mazur, Y. I.; Salamo, G. J.; Smowton, P.; Seeds, A. InAs/GaAs quantum-dot superluminescent light-emitting diode monolithically grown on a Si substrate. *ACS Photonics* **2014**, *1*, 638−642.
(25) Mazur, Y. I.; Liang, B.; Wang, Z. M.; Tarasov, G.; Guzun, D.; Salamo, G. Development of continuum states in photoluminescence of self-assembled InGaAs/GaAs quantum dots. *J. Appl. Phys.* **2007**, *101*, 014301.
(26) Mazur, Y. I.; Lopes-Oliveira, V.; de Souza, L.; Lopez-Richard, V.; Teodoro, M.; Dorogan, V.; Benamara, M.; Wu, J.; Tarasov, G.; Marega, E., Jr Carrier transfer in vertically stacked quantum ring-quantum dot chains. *J. Appl. Phys.* **2015**, *117*, 154307.
(27) Heitz, R.; Veit, M.; Ledentsov, N. N.; Hoffmann, A.; Bimberg, D.; Ustinov, V. M.; Kop'ev, P. S.; Alferov, Z. I. Energy relaxation by multiphonon processes in InAs/GaAs quantum dots. *Phys. Rev. B: Condens. Matter Mater. Phys.* **1997**, *56*, 10435.
(28) Heitz, R.; Kalburge, A.; Xie, Q.; Grundmann, M.; Chen, P.; Hoffmann, A.; Madhukar, A.; Bimberg, D. Excited states and energy relaxation in stacked InAs/GaAs quantum dots. *Phys. Rev. B: Condens. Matter Mater. Phys.* **1998**, *57*, 9050.
(29) Tang, S.; Chiang, C.; Weng, P.; Gau, Y.; Luo, J.; Yang, S.; Shih, C.; Lin, S.; Lee, S. High-temperature operation normal incident 256× 256 InAs-GaAs quantum-dot infrared photodetector focal plane array. *IEEE Photonics Technol. Lett.* **2006**, *18*, 986−988.
(30) Oktyabrsky, S.; Lamberti, M.; Tokranov, V.; Agnello, G.; Yakimov, M. Room-temperature defect tolerance of band-engineered InAs quantum dot heterostructures. *J. Appl. Phys.* **2005**, *98*, 053512.
(31) Le Ru, E.; Fack, J.; Murray, R. Temperature and excitation density dependence of the photoluminescence from annealed InAs/GaAs quantum dots. *Phys. Rev. B: Condens. Matter Mater. Phys.* **2003**, *67*, 245318.
(32) Ma, W.; Yang, X.; Chong, M.; Yang, T.; Chen, L.; Shao, J.; Lü, X.; Lu, W.; Song, C.; Liu, H. Voltage tunable two-color InAs/ GaAs quantum dot infrared photodetector. *Appl. Phys. Lett.* **2008**, *93*, 013502.

DOI: 10.1021/acsphotonics.6b00076
ACS Photonics 2016, 3, 749−753